Transworld Research Network
37/661 (2), Fort P.O., Trivandrum-695 023, Kerala, India

Electromagnetic, Magnetostatic, and Exchange-Interaction Vortices in Confined Magnetic Structures, 2008: 59-75 ISBN: 978-81-7895-373-1 Editor: E. O. Kamenetskii

4 Current induced vortex dynamics in magnetic nanodisc

Denis D. Sheka[1], Yuri Gaididei[2] and Franz G. Mertens[3]
[1]National Taras Shevchenko University of Kiev, 03127 Kiev, Ukraine; [2]Institute for Theoretical Physics, 03143 Kiev, Ukraine; [3]Physics Institute, University of Bayreuth 95440 Bayreuth, Germany

Abstract

We study the dynamics of the magnetic vortex driven by a spin current. Using a simple analytical model and numerical simulations we show that a non-decaying vortex motion can be excited by a dc spin current, whose intensity exceeds a first threshold value as a result of the balance between a spin-torque pumping and damping forces. The irreversible switching of the vortex polarity takes place for a current above a second threshold. The mechanism of the switching, which involves the process of creation and annihilation of a vortex-antivortex pair is described analytically, using a rigid model, and confirmed by detailed spin-lattice simulations.

Correspondence/Reprint request: Dr. Denis D. Sheka, National Taras Shevchenko University of Kiev, 03127 Kiev, Ukraine
E-mail: Denis_Sheka@univ.kiev.ua

1. Introduction

It is now firmly established that nonlinear excitations of soliton type play an important role in the low dimensional magnetism. Kinks in 1D magnets and localized Belavin–Polyakov solitons in 2D isotropic magnets are responsible for the destruction of long–range order at finite temperature [1]. Vortices play a similar role in 2D easy–plane magnets: the presence of vortices gives rise to the Berezinskiĭ–Kosterlitz–Thouless topological phase transition [2, 3]. 2D magnetic solitons and vortices have been studied since the end of 1970s. They are important for the dynamical and thermodynamical properties of magnets, for a review see Ref. [4, 5]. The soliton and vortex contribution to the response functions of 2D magnets has been predicted theoretically [6, 7] and observed experimentally [8, 9].

A second wind in the physics of 2D magnetic solitons and vortices appeared this decade due to the direct observation of nonlinear excitations in magnetic nanodots. Such nanodots are submicron disk–shaped particles, which have a single vortex in the ground state due to the competition between exchange and magnetic dipole–dipole interaction [10, 11]. A vortex state is obtained in nanodots that are larger than a single domain particle whose size is a few nanometers: e.g. for the permalloy (Py, $Ni_{80}Fe_{20}$) nanodot the exchange length $\ell \sim 6nm$. The vortex state of magnetic nanodots has drawn much attention because it could be used for high-density magnetic storage and miniature sensors [11, 12]. For this one needs to control magnetization reversal, a process where vortices play a crucial role [13]. Notable experiments with magnetic force microscopy on circular nanoscale Py dots [14–19], and polycrystalline Co [20–22] disposed in arrays over nanopatterned films, report images of vortex cores, where the magnetization is deviated out of the plane of the film. Lorentz transmission electron microscopy imaging and micro Hall magnetometry also show vortices to be favorable configurations in permalloy nanodisks [17, 21, 23]. Great progress has been made recently with the possibility to observe high frequency dynamical properties of the vortex state magnetic dots by Brillouin light scattering of spin waves [24, 25], time–resolved Kerr microscopy [19], phase sensitive Fourier transformation technique [26], and X–ray imaging technique [27]. This kind of experiments is opening the door to direct theoretical investigations of soliton and vortices in ferromagnetic materials, with the aim to understand the interplay between mesoscopic nonlinear collective excitations and geometrical constraints, like shape, size and boundary conditions at the interfaces, see Ref. [10].

The control of magnetic nonlinear structures using an electrical current is of special interest for applications in spintronics [28, 29]. The spin torque effect, which is the change of magnetization due to the interaction with an electrical current, was predicted by Slonczewski [30] and Berger [31] in 1996. During the last decade this effect was tested in different magnetic systems [32–34] and nowadays it plays an important role in spintronics [28, 35]. Recently the spin torque effect was observed in vortex state nanoparticles. In particular, circular vortex motion can be excited by an AC [36] or a DC [37] spin-polarized current. Very recently it was predicted theoretically [38, 39] and observed experimentally [40] that the vortex polarity can be controlled using a spin-polarized current. This opens up the possibility of realizing electrically controlled magnetic devices, changing the direction of modern spintronics [41].

There exist two main kinds of heterostructures, where the spin-torque effect is observed [42]: a current-in-plane (CIP) structure, where both polarizer and sensor layer are magnetized in plane and a current-perpendicular-to-the plane (CPP) structure, where the sensor is in-plane magnetized, while the polarizer is magnetized perpendicular to the plane. In this paper we consider the CPP heterostructure, which is more efficient [43]. A typical CPP heterostructure with a vortex state sensor was proposed recently in Refs. [38, 39].

It is well-known [30] that the spin torque effect causes a spin precession in a homogeneously magnetized particle. A similar picture also takes place for the vortex state Heisenberg system [38], where the spin current, which is perpendicular to the nanoparticle plane, mainly acts like an effective perpendicular DC magnetic field. Recently we have shown [39] that the dipolar interaction crucially changes the physical picture of the process. The precessional vortex state [38] becomes unfavorable, because the dipolar interaction tries to minimize the edge surface magnetostatic charges, hence the magnetization at the dot edge is almost conserved [44]. In this paper, by using the rigid vortex approach, we show that the spin current causes a nontrivial vortex dynamics. When the current strength exceeds some threshold value j_{cr}, the vortex starts to move along a spiral trajectory, which converges to a circular limit cycle. When the current strength exceeds the second threshold value j_{sw}, the vortex switches its polarity during its spiral motion. After that it rapidly goes back to the dot center. We present a simple picture of this switching process and confirm our results by spin-lattice simulations.

We consider a pillar structure [38, 45, 46], in which the magnetization direction in the polarizer is aligned parallel to z (see Fig. 1). An electrical current is injected in the polarizer, where it is polarized along σ (which is collinear to z in our case). The sensor is a thin disk with a vortex ground state: the magnetization lies in the disk plane in the main part of the disk being parallel to the disk edge, however in the disk center the magnetization becomes perpendicular to the disk plane in order to prevent a singularity in the magnetization distribution [5, 10]. This perpendicular magnetization distribution forms the vortex core, which is oriented along z or opposite to z. Such a direction of the core magnetization is characterized by the vortex polarity ($p = +1$ or $p = -1$, respectively). In the pillar stack, the

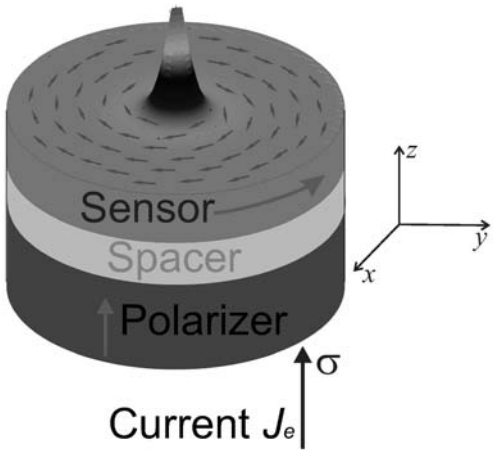

Figure 1. Schematic of the heterostructure.

thickness of the nonmagnetic layer (spacer) is much less than the spin diffusion length [45, 47], hence the spin polarization of the current is conserved when it flows into the sensor.

2. The model

We start from the model of the ferromagnetic system with the Heisenberg exchange and dipolar interaction [48]:

$$\mathcal{H} = -\frac{JS^2}{2}\sum_{(n,\delta)} \boldsymbol{S}_{\boldsymbol{n}}\cdot\boldsymbol{S}_{\boldsymbol{n}+\boldsymbol{\delta}} + \frac{D}{2}\sum_{\substack{n,n'\\ n\neq n'}} \frac{\boldsymbol{S}_{\boldsymbol{n}}\cdot\boldsymbol{S}_{\boldsymbol{n}'} - 3\,(\boldsymbol{S}_{\boldsymbol{n}}\cdot\boldsymbol{e}_{\boldsymbol{n}\boldsymbol{n}'})\,(\boldsymbol{S}_{\boldsymbol{n}'}\cdot\boldsymbol{e}_{\boldsymbol{n}\boldsymbol{n}'})}{|\boldsymbol{n}-\boldsymbol{n}'|^3}. \tag{1}$$

Here $\boldsymbol{S}_{\boldsymbol{n}} \equiv (S^x_{\boldsymbol{n}}, S^y_{\boldsymbol{n}}, S^z_{\boldsymbol{n}})$ is a classical spin vector with fixed length S on the site $n = (n_x, n_y, n_z)$ of a three–dimensional cubic lattice with integers n_x, n_y, n_z, J is the exchange integral, the parameter $D = \mu_B^2 g^2/a^3$ is the strength of the long–range dipolar interaction, g is the Landé–factor, a is the lattice constant; the vector δ connects nearest neighbors, and $\boldsymbol{e}_{\boldsymbol{n}\boldsymbol{n}'} \equiv (\boldsymbol{n}-\boldsymbol{n}')/|\boldsymbol{n}-\boldsymbol{n}'|$ is a unit vector.

The spin dynamics of the system is described by the discrete version of the Landau–Lifshitz–Gilbert equation with account of the spin–torque effect by a Slonczewski–Berger term [30, 31]:

$$\frac{\mathrm{d}\boldsymbol{S}_{\boldsymbol{n}}}{\mathrm{d}t} = -\frac{1}{\hbar}\left[\boldsymbol{S}_{\boldsymbol{n}}\times\frac{\partial\mathcal{H}}{\partial\boldsymbol{S}_{\boldsymbol{n}}}\right] - \frac{\alpha}{S}\left[\boldsymbol{S}_{\boldsymbol{n}}\times\frac{\mathrm{d}\boldsymbol{S}_{\boldsymbol{n}}}{\mathrm{d}t}\right] + \boldsymbol{T}_{\boldsymbol{n}}, \tag{2a}$$

where the second term on the righthand side describes the spin relaxation with the damping coefficient α. The last term comes from the spin-torque effect: when a current flows perpendicular to the plane of the nanoparticle (thickness h), which is characterized by the spin polarization unit vector $\boldsymbol{\sigma}$ (along z in our case), the spin torque reads:

$$\boldsymbol{T}_{\boldsymbol{n}} = \frac{j\mathcal{A}/\hbar}{S + \mathcal{B}\boldsymbol{S}_{\boldsymbol{n}}\cdot\boldsymbol{\sigma}}\Big[\boldsymbol{S}_{\boldsymbol{n}}\times\big[\boldsymbol{S}_{\boldsymbol{n}}\times\boldsymbol{\sigma}\big]\Big], \quad \mathcal{A} = \frac{4\eta_{sp}^{3/2}}{3(1+\eta_{sp})^3 - 16\eta_{sp}^{3/2}},\ \mathcal{B} = \frac{(1+\eta_{sp})^3}{3(1+\eta_{sp})^3 - 16\eta_{sp}^{3/2}}. \tag{2b}$$

Here $j = J_e/J_p$ is the normalized spin current, J_e is the electrical current density, $J_p = \mu_0 M_S^2 |e| h/\hbar$, where $M_S = g\mu_B S/a^3$ is the saturation magnetization, e is the electron charge, and μ_0 is the vacuum permeability, and $\eta_{sp} \in (0;1)$ is the degree of spin polarization.

In the continuum description, the spin dynamics is described by a magnetization unit vector $\boldsymbol{m} = -\langle S_{\boldsymbol{n}}\rangle$. The continuum version of the Hamiltonian (1), the energy functional E reads:

$$E = \int \mathrm{d}^3x \left[\frac{A}{2}(\boldsymbol{\nabla}\boldsymbol{m})^2 - \frac{M_S}{2}(\boldsymbol{m}\cdot\boldsymbol{H}_m)\right], \tag{3}$$

where $A = JM_S^2 a^5/D$ is the exchange constant and H_m is the magnetostatic field, which comes from the dipolar interaction [48]. The continuum limit becomes adequate, when the typical exchange length

$$\ell = a\sqrt{\frac{Ja^3}{4\pi D}} = \sqrt{\frac{A}{4\pi M_S^2}} \tag{4}$$

is larger than the lattice constant a.

Using the angular parametrization $m = (\sin\theta\cos\phi;\ \sin\theta\sin\phi;\ \cos\theta)$, one can write down the continuum version of the Landau-Lifshitz Eq. (2) with the Slonczewski–Berger term in the form:

$$\sin\theta\partial_\tau\phi = -\frac{\delta\mathscr{E}}{\delta\theta} - \alpha\partial_\tau\theta, \tag{5b}$$

$$-\sin\theta\partial_\tau\theta = -\frac{\delta\mathscr{E}}{\delta\phi} - \alpha\sin^2\theta\partial_\tau\phi + \frac{\varkappa\sin^2\theta}{1+\mathcal{B}\sigma\cos\theta}, \tag{5a}$$

Here and below we use the dimensionless variables:

$$\tau = \omega_0 t,\ \boldsymbol{\xi} = \frac{\boldsymbol{r}}{\ell},\ \mathscr{E} = \frac{E}{4\pi M_S^2},\ \varkappa = \frac{j\sigma\mathcal{A}}{\omega_0},\ \omega_0 = 4\pi\gamma M_S. \tag{6}$$

where γ is the gyromagnetic ratio. Note that we are interested here only in the influence of the homogeneous spin torque $T \propto \boldsymbol{j}\cdot\boldsymbol{m}$. Such an approach works if the magnetization does not change in the direction of the current propagation $(\ell|\partial_z\boldsymbol{m}| \ll 1)$, which is reasonable for the perpendicular current and thin nanodisks. However, if one applies a current in the direction of the disk plane, there appears a nonhomogeneous spin torque $T \propto (\boldsymbol{j}\cdot\boldsymbol{\nabla})\boldsymbol{m}$[49], which causes another mechanism of the vortex dynamics [36, 40, 41, 50, 51].

3. Stationary states

Let us consider a disk–shape particle of the radius L and the thickness h. For the small size nanoparticle the ground state is uniform; it depends on the particle aspect ratio $\varepsilon = h/2L$: thin nanodisks are magnetized in the plane (when $\varepsilon < \varepsilon_c \approx 0{:}906$ [52]) and thick ones along the axis (when $\varepsilon > \varepsilon_c$). Under the influence of the spin current the homogeneous ground state of the system changes: there appears a dynamical cone state with the out-of-plane magnetization $\cos\theta_0 \approx \varkappa/\alpha$, see Ref. [38]. In this state all spins precess with the frequency $\Omega_0 \equiv \partial_\tau\phi \approx \varkappa/\alpha$, where we have neglected here the B–term for simplicity.

When the particle size exceeds some critical value, typically $(3-4)\ \ell$ [53], the magnetization curling becomes energetically preferable due to the competition between the exchange and dipolar interaction. For the disk shape particle there appears the vortex state. For thin enough disks the vortex structure does not depend on the z-coordinate of the disk and the magnetization distribution for the vortex, which is situated in the disk center, is determined by the expressions [5]

$$\cos\theta = pf(|\zeta|), \qquad \phi = q\arg\zeta + C\pi/2. \tag{7}$$

Here $\zeta = x + \imath y$ is the coordinate in the disk plane, q = +1 is the vortex π_1 topological charge (vorticity), $C = \pm 1$ characterizes the vortex chirality, and $p = \pm 1$ determines the direction of the vortex core magnetization (polarity). The bell-shaped function $f(|\zeta|)$ describes the vortex core magnetization. The vortex polarity is connected to the π_2 topological properties of the vortex, namely, to the Pontryagin index

$$Q = \frac{1}{4\pi}\int \mathrm{d}^2x\Omega, \quad \Omega = \epsilon_{ij}\sin\theta\partial_i\theta\partial_j\phi. \tag{8}$$

For the vortex configuration the Pontryagin index takes the half-integer values $Q = pq/2$.

For the vortex solution localized at $Z = X + \imath Y = R\exp(\imath\Phi)$, the ϕ-field has the form $\phi = q\arg(\zeta - Z) + C\pi/2$: Such a form of the ϕ–field satisfies the Laplace equation, so it describes the planar vortex dynamics (neglecting the z-component of magnetization) for the infinite Heisenberg magnets. The finite size effects for the circular Heisenberg magnet can be described by the image-vortex ansatz [5]. Besides one has to take into account the long-range dipolar interaction, which leads in general to integro-differential equations [54]. For a thin ferromagnet the dipolar interaction produces two main effects [55]: (i) an effective uniaxial anisotropy of the easyplane type caused by the faces surface magnetostatic charges and (ii) an effective in-plane anisotropy caused by the edge surface charges (surface anisotropy). Due to the surface anisotropy the magnetization near the disk edge is constrained to be tangential to the boundary, which prevents its precession near the edge (absence of surface charges). This conclusion about effective fixed (Dirichlet) boundary conditions for thin vortex state nanodisks agrees with results of linear analysis [44, 56]. Finally, the ϕ–field can be written in the form

$$\phi = \arg\left[\zeta - Z\right] + q_I\arg\left[\zeta - Z_I\right] - q_I\arg Z + C\frac{\pi}{2}. \tag{9}$$

Here $Z_I = ZL^2/R^2$ is the "image" vortex coordinate and q_I = +1 is the "image" vortex vorticity; the "image" vortex is added to satisfy the Dirichlet boundary conditions.

4. Rigid vortex dynamics without a spin–torque

It is well-known that the vortex behaves like a particle under weak external influences. In particular, if an external DC magnetic field is applied in the disk plane, the vortex starts to gyrate [27, 57]. This rigid vortex dynamics can be well-described using a Thiele approach [58, 59]. Following this approach we construct a force balance equation. Taking Eq. (5a) times $\nabla\theta$ and Eq. (5b) times $\nabla\phi$, summing the two equations and integrating the result over the system volume gives a force balance equation

$$\boldsymbol{F}^{\mathrm{gyro}} + \boldsymbol{F}^{\mathrm{dis}} + \boldsymbol{F}^{\mathrm{ext}} = 0. \tag{10}$$

Here $\boldsymbol{F}^{\mathrm{gyro}} = \int \mathrm{d}^3\sin\theta\left(\partial_\tau\phi\nabla\theta - \partial_\tau\theta\nabla\phi\right)$ is a gyroscopical force, $\boldsymbol{F}^{\mathrm{dis}} = \alpha\int \mathrm{d}^3x\left(\partial_\tau\theta\nabla\theta + \sin^2\theta\partial_\tau\phi\nabla\phi\right)$ is a dissipative force, and $\boldsymbol{F}^{\mathrm{ext}} = \int \mathrm{d}^3x\left(\frac{\delta\mathscr{E}}{\delta\theta}\nabla\theta + \frac{\delta\mathscr{E}}{\delta\phi}\nabla\phi\right)$ is an external force.

In a Thiele approach, the vortex moves as a rigid particle without changing its shape. Therefore we can combine our image-vortex ansatz together with a travelling wave ansatz [5]:

$$\cos\theta(\zeta,\tau) = pf\big[\zeta - Z(\tau)\big],$$

$$\phi(\zeta,\tau) = \arg\big[\zeta - Z(\tau)\big] + q_I \arg\big[\zeta - Z_I(\tau)\big] - q_I \arg Z(\tau) + C\frac{\pi}{2}. \tag{11}$$

Now we are able to calculate the forces in a standard way. The gyroscopical force

$$\boldsymbol{F}^{\text{gyro}} = Gh\left[\dot{\boldsymbol{R}} \times \boldsymbol{e}_z\right], \qquad G = -4\pi Q, \tag{12}$$

where G is the gyroconstant (for the vortex $G = -2\pi p$) [60, 61] and $R = (X, Y)$. The dissipative force $F^{\text{dis}} = -2\pi\eta h\dot{\boldsymbol{R}}$ with $\eta \approx (\alpha/2)\ln(L/\ell)$. Thus the Thiele equations (10) reads:

$$Gh\left[\dot{\boldsymbol{R}} \times \boldsymbol{e}_z\right] - 2\pi\eta h\dot{\boldsymbol{R}} + \boldsymbol{F}^{\text{ext}} = 0. \tag{13}$$

The external force, acting on the vortex, $\boldsymbol{F}^{\text{ext}} = -\nabla_{\boldsymbol{R}}\mathscr{E}$, where the total energy is described by Eq. (3). The main contribution to this energy is caused by the magnetostatic energy of volume charges

$$\mathscr{E}^m = \frac{1}{8\pi}\int \mathrm{d}\boldsymbol{r}\int \mathrm{d}\boldsymbol{r}'\frac{\varrho(\boldsymbol{r},\boldsymbol{Z})\varrho(\boldsymbol{r}',\boldsymbol{Z})}{|\boldsymbol{r}-\boldsymbol{r}'|}, \tag{14}$$

where $\varrho = \nabla \cdot \boldsymbol{m}$ is the density of volume charges and $\boldsymbol{r} = (x, y, z)$.

For small displacements of the vortex center from the origin ($\Delta = R/L \ll 1$), one can use a Taylor series expansion [62, 63]. In the lowest approximation $\mathscr{E} = \mathscr{E}_0 + kR^2/2$, and the restoring force $F^{\text{ext}} = -kh\boldsymbol{R}$. Therefore the Thiele–like equation (13) results in a vortex gyration: the vortex precesses with the eigenfrequency $\Omega_G = k/|G|$. For small aspect ratios $\varepsilon \ll 1$ this gyrofrequency can be approximately described analytically, $\Omega_G = 10\varepsilon/9\pi$ [64]. For finite ε one can use the analysis in [65, 66]. For larger displacements one can use the next Taylor expansion term [63], and the analysis can be done numerically only. Instead, we can extract the information from the simulation data in a wide range of the vortex displacement Δ. The details of simulations are described in Sec. 6. In the Fig. 2 we have plotted the numerical data for the energy

$$W = \frac{\mathscr{E} - \mathscr{E}_0}{\pi L^2 h\Omega_G(\varepsilon)} \tag{15}$$

as a function of the vortex displacement Δ for different thicknesses h of the disk. Here $\Omega_G(\varepsilon)$ is the vortex eigenfrequency for small vortex shifts, which agrees with results in Refs. [65, 66]. By analyzing the numerical data one can approximately restore the shape of the total energy of the system by fitting:

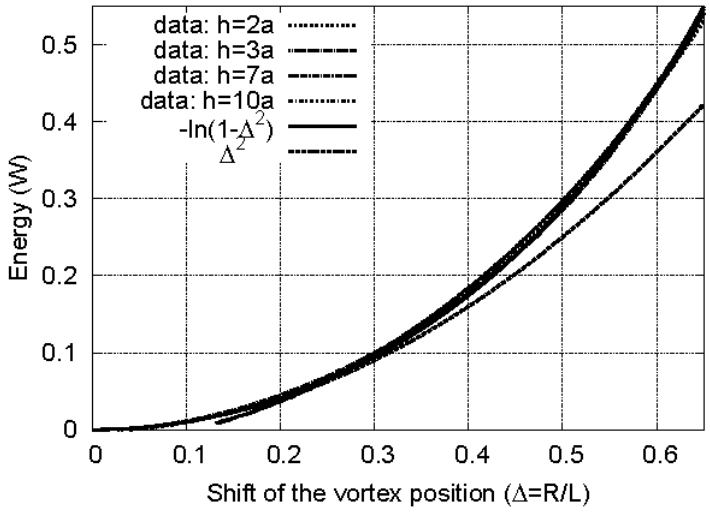

Figure 2. Energy of the vortex (15) *vs.* the vortex displacement Δ from simulations on disks with the diameter $2L = 40a$ and different thicknesses h, $\ell = 1.3a_0$, $\alpha = 0.01$.

$$\mathscr{E} \approx \mathscr{E}_0 - \pi L^2 h \Omega_G(\varepsilon) \ln\left(1 - \Delta^2\right). \tag{16}$$

Finally, the external force

$$\boldsymbol{F}^{\text{ext}} = -k(\Delta) h \boldsymbol{R}, \qquad k(\Delta) \approx \frac{2\pi\Omega_G(\varepsilon)}{1-\Delta^2}. \tag{17}$$

5. Spin–torque effect in the vortex dynamics

Let us apply a spin current to the system. One can suppose that a rigid vortex approach still works correctly in the case of a weak current. Using the same procedure as in the previous section, one can derive the force balance equation. It has a form similar to (13). However, in addition to the external dipolar force F^{ext} there appears a new force

$$\boldsymbol{F}^{\text{cur}} = -\varkappa \int \mathrm{d}^3x \frac{\sin^2\theta}{1 + \mathcal{B}\sigma\cos\theta} \boldsymbol{\nabla}\phi, \tag{18}$$

which is caused by the spin torque effect. For the analytical treatment of this force one can neglect the $\mathcal{B}$-term in the denominator and use the ansatz (11), which leads to the force [67, 68]:

$$\boldsymbol{F}^{\text{cur}} \approx -\varkappa \int \mathrm{d}^3x \boldsymbol{\nabla}\phi = -\pi\varkappa q h \left[\boldsymbol{R} \times \boldsymbol{e}_z\right], \tag{19}$$

where the vortex position $\boldsymbol{R}$ is measured from the disk center.

Finally the force balance condition (10) takes the form of a Thiele–like equation, which describes the vortex dynamics as a rigid particle

$$G\left[\dot{\boldsymbol{R}}\times\boldsymbol{e}_z\right]=2\pi\eta\dot{\boldsymbol{R}}+k(\Delta)\boldsymbol{R}+\pi\varkappa\left[\boldsymbol{R}\times\boldsymbol{e}_z\right]. \tag{20}$$

The vector equation (20) can be presented also in the scalar form

$$\dot{\Phi}=\frac{p}{2\pi}k(\Delta)-2\pi\eta\frac{\dot{R}}{R},\qquad \frac{\dot{R}}{R}=-\eta p\dot{\Phi}-\frac{1}{2}\varkappa p. \tag{21}$$

Without the spin current term the vortex stays at the disk center, which is a ground state. This stability of the origin is provided by the damping. However, the loss of energy due to the damping can be compensated by the energy pumping due to the spin current if the current exceeds a critical value, see below. One can see from Eqs. (21) that the vortex position at origin can be unstable when $p\varkappa<0$. The spin current excites a spiral vortex motion, which finally leads to the circular limit cycle $Z(\tau)=R\exp(i\Omega\tau)$

$$\Omega=\frac{pk(\Delta)}{2\pi}=-\frac{\varkappa}{2\eta}. \tag{22}$$

The critical current can be easily estimated from the main term expansion at $\Delta=0$:

$$\varkappa_{\rm cr}=2\eta\Omega_G(\varepsilon),\quad j_{\rm cr}=\frac{2\eta\Omega_G(\varepsilon)\omega_0}{\mathcal{A}}. \tag{23}$$

The spiral vortex motion can be excited under the conditions: $|j|>j_{\rm cr}$ and $pj\sigma<0$. Note that for small aspect ratios

$$j_{\rm cr}\approx\frac{5\omega_0\alpha h}{9\pi\mathcal{A}L}\ln\frac{L}{\ell}. \tag{24}$$

The radius of this limit cycle can be found by solving the equation $k(R/L)/k(0)=|j|/j_{\rm cr}$. Using (17), one can find the approximate dependence

$$R=L\sqrt{1-\frac{j_{\rm cr}}{|j|}}. \tag{25}$$

Note that a similar threshold dependence was obtained recently by Ivanov and Zaspel [68] using a linear mode analysis: $R=0.153L\sqrt{(j-j_c)/j_c}$.

6. Numerical simulations

In order to check these predictions about the vortex dynamics, we have performed numerical simulations of the discrete (spin lattice) version of the Landau-Lifshitz equations with the spin torque term in the form (2). Our main assumption is that $\boldsymbol{S}_n$ depends only on x and y coordinates. Such a plane–parallel spin distribution is adequate for thin nanoparticles. In this case the energy (1) can be presented in the form [55]

$$\mathcal{H}=-\frac{Jh}{2a_0}\sum_{\langle\nu,\nu'\rangle}\boldsymbol{S}_\nu\boldsymbol{S}_{\nu'}-\frac{D}{2}\sum_{\nu,\mu}\left[C^1_{\mu\nu}\left(\boldsymbol{S}_\nu\cdot\boldsymbol{S}_\mu-3S^z_\nu S^z_\mu\right)+C^2_{\mu\nu}\left(S^x_\nu S^x_\mu-S^y_\nu S^y_\mu\right)+C^3_{\mu\nu}\left(S^x_\nu S^y_\mu+S^y_\nu S^x_\mu\right)\right].$$

Here the sum runs only over the 2D lattice. All information about the original 3D structure of our system is in the coefficients $C^k_{\mu\nu} = \sum_{\substack{m_z,n_z \\ r_{nm}\neq 0}} \mathcal{C}_k/(2r^5_{mn})$ with $\mathcal{C}_1 = r^2_{mn} - 3z^2_{mn}$, $\mathcal{C}_2 = 2(x^2_{mn} - y^2_{mn})$, $\mathcal{C}_3 = 6x_{mn}y_{mn}$.

Numerically we have integrated the discrete spin-lattice Eqs. (2) over a square lattice of size $(2L)^2$ using the fourth-order Runge-Kutta scheme with the time step $\Delta\tau = 0.01$. Each lattice is bounded by the circle of radius L.

First we have performed a series of simulations without a spin current with a shifted vortex in order to treat the case of a restoring force (17). Initially we shifted a vortex by a distance $\Delta = R/L$, using the analytical ansatz (9). Since it gives an approximate solution only, we run simulations for a short time for the overdamped system (we used $\alpha \lesssim 0.5$). This was enough to let the vortex adapt to the lattice and to damp out all spin waves which resulted from the not perfect initial spin distribution. After that we started simulations with the nominal damping constant. During its dynamics the vortex moves along the spiral trajectory in agreement with Eq. (13) and rapidly reaches the center of the disk. By analyzing the simulation data we calculated the total energy of the vortex state nanodisk as a function of the vortex shift Δ. We found that in a wide range of parameters the normalized energy (15) can be fitted with high accuracy as $W = -\ln(1 - \Delta^2)$, see Fig. 2. Note that such a dependence does not depend on the way how we shift the vortex: these results agree with data for the vortex dynamics caused by a spin-torque. It is instructive also to note that the dependence $\mathscr{E}(\Delta)$, see Eq. 16, functionally coincides with the 2D Coulomb interaction of the vortex with its image [5].

Let us consider now the influence of a spin-torque on the vortex dynamics. The vortex dynamics results from the force balance between a driving force (by the current), a dipolar force, a gyroscopical force, and a dissipative force. In the simulations we observe that when the vortex and the spin-current have the same polarization ($j\sigma p > 0$) the vortex does not quit the center of the disk. However, for $j\sigma p < 0$ ($p = +1$, $\sigma = +1$ and $j < 0$ in our case) the vortex under the action of the current starts to move out of the disk center following a spiral trajectory. The spiral type of motion is caused by the gyroscopical force, which acts on a moving vortex perpendicular to its velocity in the same way as the Lorentz force acts on a charged particle in a magnetic field. The role of the charge plays the π_2 topological charge Q, see Eq. (8). The sign of Q determines the direction of the vortex motion, which is clockwise for $p = +1$. Under the action of the current the vortex moves along the spiral trajectory starting from the disk center and finally reaches a circular limit cycle, see Fig. 3. The vortex motion can be excited only if the current exceeds the critical value j_{cr}, see Fig. 4. Numerically we found that the threshold value $j_{cr} = 0.0165$, which corresponds to $\varkappa_{cr} = 7.94 \times 10^{-4}$. This is in a good agreement with out theoretical analysis $\varkappa_{cr} = 7.96 \times 10^{-4}$, which results from Eq. (23).

The radius of the vortex limit trajectory increases with the current strength, in agreement with (25). At some value, the radius becomes comparable with the system size L and the vortex dynamics becomes nonlocal. Finally it results in a switching of the vortex core, see [39]. In the next section we present a detailed study of the switching mechanism.

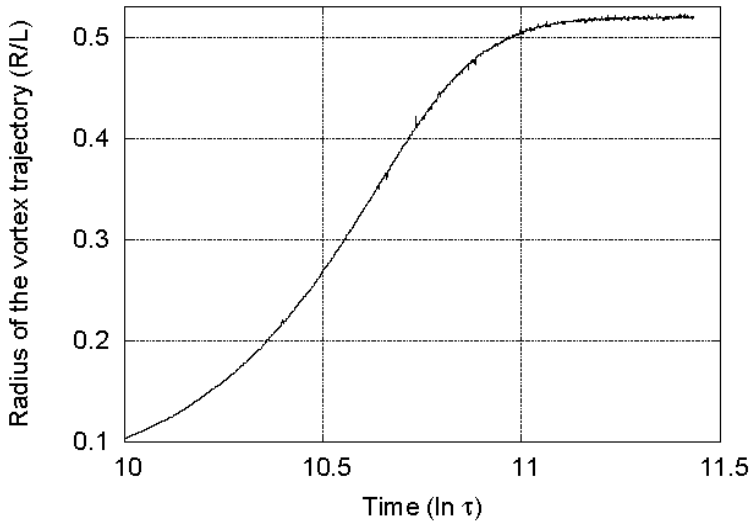

Figure 3. Limit cycle in the vortex trajectory from the simulations for $j = -0.055$, which corresponds to $\varkappa = 0.015$. Other system parameters: $2L = 50a$, $h = 5a$, $\ell = 1.3a$, $\alpha = 0.01$, $\sigma = 1$ and $\eta_{sp} = 0.26$.

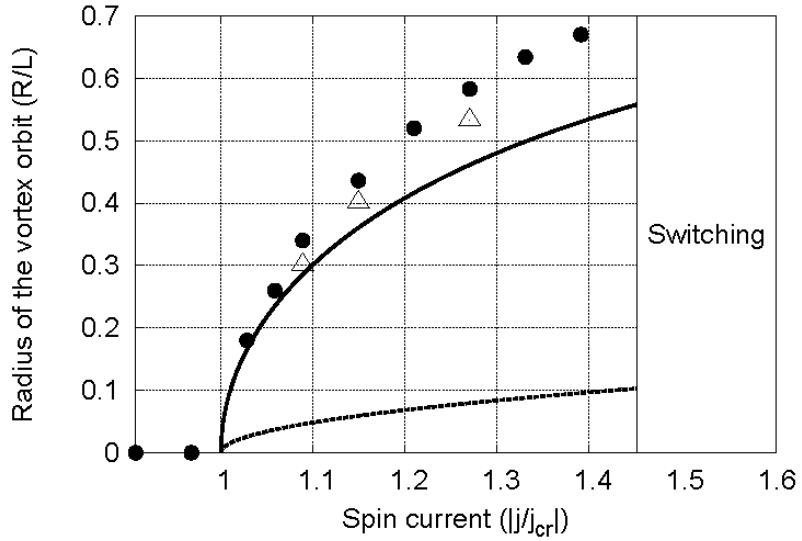

Figure 4. Radius of the vortex for the disk with $2L = 50a$, $h = 5a$, $\ell = 1.3a$, $\alpha = 0.01$, $\sigma = -1$ and $\eta_{sp} = 0.26$. Symbols present simulations data: ● for the original system and Δ for the simplified one with $\mathscr{B} = 0$; the solid curve is the dependence (25); the dashed curve is the analytical result from Ref. [68].

7. Switching of the vortex polarity

The switching of the vortex polarity in a vortex state nanodot is the subject of different studies. The mechanism of the vortex switching is essentially the same in all systems where the switching was observed [39, 40, 67, 69–73]. Under the action of the spin current, the vortex, originally situated in the disk center [see Fig. 5(b)], moves along the spiral trajectory, in the counterclockwise direction in our case, see Fig. 5(a). The moving vortex excites a non-symmetric magnon mode with a dip situated towards the disk center, see Fig. 5(c). When the vortex (V) moves away from the center, the amplitude of the dip increases, see Fig. 5(d); if the current is so strong that the dip can reach a minimum ($\theta = \pi$, i.e. $m_z = -1$), a pair of a new vortex (NV) and antivortex (AV) is created, see Fig. 5(e). The reason why the new-born vortex tears off his partner has a topological origin. The gyroscopic force depends on the total topological charge Q, see Eq. (12). Therefore it produces a *clockwise* motion for the original vortex ($q_V = 1$, $p_V = 1$, $Q_V = 1/2$) and the new-born antivortex ($q_{AV} = -1$; $p_{AV} = -1$; $Q_{AV} = -1/2$) while the new-born vortex ($q_{NV} = -1$, $p_{AV} = 1$, $Q_{NV} = -1/2$) moves in the *anti-clockwise* direction. As a result the new vortex separates from the vortex-antivortex pair and rapidly moves to the origin, see Figs. 5(e) and 5(a). The attractive force between the original vortex ($q = 1$) and the antivortex ($q = -1$) facilitates a binding and subsequent annihilation of the vortex-antivortex pair, see Fig. 5(d). This three–body process in a no-driving case is studied in details by Komineas and Papanicolaou in another chapter of this volume [74]. During the collision, the original vortex and the antivortex form a topological nontrivial pair ($Q = 1$), which performs a rotational motion around some guiding center [75]. This rotating vortex dipole forms a localized skyrmion (Belavin-Polyakov soliton [76]), which is stable in the continuum system. In the discrete lattice system the radius of this soliton, i.e. the distance between the vortex and antivortex, rapidly decreases almost without energy loss. When the soliton radius is about the lattice constant, it vanishes [73, 75]; this vanishing is accompanied by strong spin-wave radiation, because the topological properties of the system change [77, 78].

In order to describe analytically the three–body problem we use the rigid approach, based on Thiele-like equations (20):

$$-2\pi q_i p_i \left[\dot{\boldsymbol{R}}_i \times \boldsymbol{e}_z\right] = 2\pi\eta\dot{\boldsymbol{R}}_i + \frac{2\pi\Omega_G}{1 - R_i^2/L^2}\boldsymbol{R}_i - \frac{\partial \mathscr{E}^{\text{int}}}{\partial \boldsymbol{R}_i} + \pi\varkappa q_i\left[\boldsymbol{R}_i \times \boldsymbol{e}_z\right], \quad i = 1, 2, 3. \tag{26}$$

Here the additional energy

$$\mathscr{E}^{\text{int}} = 2\pi\ell^2 \sum_{j\neq i} q_i q_j \ln\left(\frac{|\boldsymbol{R}_i - \boldsymbol{R}_j|}{\ell}\right), \quad i = 1, 2, 3 \tag{27}$$

describes the 2D Coulomb interaction between different vortices. To integrate numerically the differential algebraic system (26), one needs to solve at each step a linear system; we used the MAPLE software [79], which includes such a facility. The set of Eqs. (26) describes the main features of the observed three–body dynamics. In Fig. 6 we present a numerical solution of Eq. (26) for parameters which are similar to our simulations [Fig. 5]. During the evolution, the original vortex and the antivortex create a

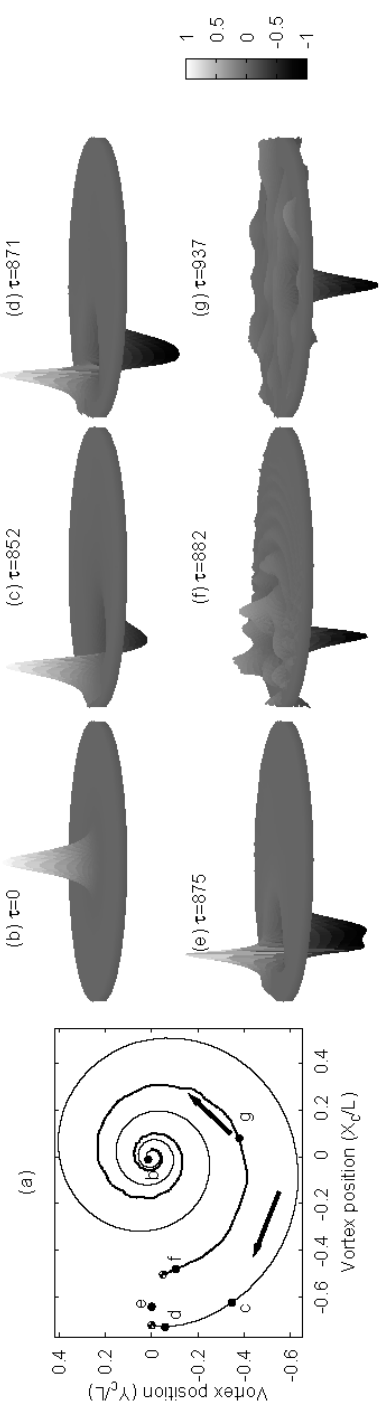

Figure 5. Temporal evolution of the switching process from simulations for the vortex state disk with $2L = 100a$, $h = 10a$, $\ell = 2.65a$, 0.01, $\sigma = -1$ and $\eta_{sp} = 0.26$. (a) The vortex trajectory. [(b)-(f)] Snapshot images illustrating the three-dimensional distribution of magnetization z component. The current $j = -0.1$, which corresponds to $\aleph = -0.027$.

rotating dipole, in agrement with Refs. [74, 75], which moves along some main trajectory. The distance in this vortex dipole rapidly tends to zero with a typical time τ of about 10 [Fig. 6(a)] in our case in agreement with the simulation data [Fig. 5]. The new–born vortex moves in the clockwise direction to the origin, following a spiral trajectory [Fig. 6(b)].

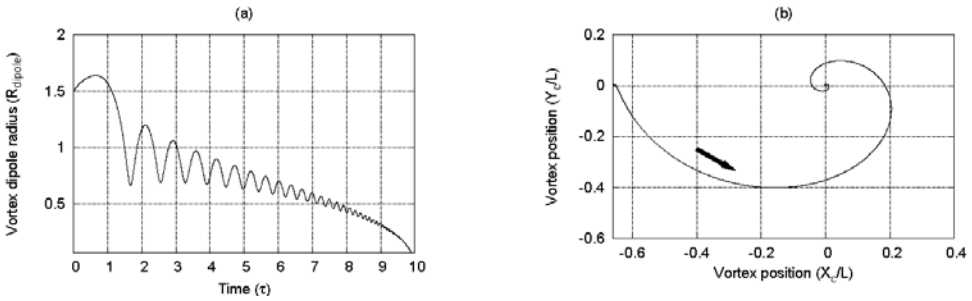

Figure 6. Numerical solution of Eqs. (26) for the system with $2L = 100a$, $\ell = 2.65a$, $\alpha = 0.01$, $\varkappa = -0.027$, and $\Omega_G = 0.0287$. The original vortex was situated at $(-36a, 0)$, the antivortex at $(-34.5a, 0)$, and the newborn vortex at $(-33a, 0)$. (a) The distance between the original vortex and the antivortex (vortex dipole radius $R_{\text{dipole}} = |R_V - R_{AV}|$ as a function of dimensionless time τ; (b) the trajectory of the new-born vortex.

8. Summary

To summarize, we have studied the magnetic vortex dynamics under the action of an electrical current. The steadystate vortex motion (circular limit cycle) can be excited due spin–transfer effect above a threshold current. This limit cycle results from the balance of forces between the pumping (due to the spin-torque effect) and damping (due to the Gilbert relaxation) [67, 68]. For a stronger current the switching of the vortex polarity takes place. It is important to stress that such a switching picture involving the creation and annihilation of a vortex-antivortex pair seems to be very general and does not depend on the details how the vortex dynamics was excited. In particular, such a switching mechanism can be induced by a field pulse [69–71], by an AC oscillating [72] or rotating field [73], by an in-plane electrical current (nonhomogeneous spin torque) [40, 51] and by a perpendicular current (our case, the homogeneous spin torque) [39, 67, 68]. Our analytical analysis is confirmed by numerical spin-lattice simulations.

Authors acknowledge support from the Deutsches Zentrum für Luft- und Raumfart e.V., Internationales Büro des Bundesministeriums für Forschung und Technologie, Bonn, in the frame of a bilateral scientific cooperation between Ukraine and Germany, project No. UKR 05/055. D.D.S. and Yu.G. thank the University of Bayreuth, where a part of this work was performed, for kind hospitality. Yu. G. acknowledges support from the Special Program of Department of Physics and Astronomy of the National Academy of Sciences of Ukraine. D.D.S. acknowledges support from the Alexander von Humboldt–Foundation and the grant No. F25.2/098 from the Fundamental Researches State Fund of Ukraine.

References

1. V. G. Bar'yakhtar and B. A. Ivanov, Sov. Sci. Rev. Sec.A. **16**, 3 (1993).
2. V. L. Berezinskiĭ, Sov. Phys JETP **34**, 610 (1972).
3. J. M. Kosterlitz and D. J. Thouless, J. Phys. **C 6**, 1181 (1973).
4. A. M. Kosevich, B. A. Ivanov, and A. S. Kovalev, Physics Reports **194**, 117 (1990), URL http://www.sciencedirect.com/science/article/B6TVP-46SXP0P-19/2/d0a99bbbccf078602123-db3e5d601202.
5. F. G. Mertens and A. R. Bishop, in *Nonlinear Science at the Dawn of the 21th Century*, edited by P. L. Christiansen, M. P. Soerensen, and A. C. Scott (Springer–Verlag, Berlin, 2000).
6. F. G. Mertens, A. R. Bishop, G. M. Wysin, and C. Kawabata, Phys. Rev. B **39**, 591 (1989), URL http://link.aps.org/abstract/PRB/v39/p591.
7. B. A. Ivanov and A. K. Kolezhuk, Low Temp. Phys. **21 (4)**, 275 (1995).
8. D. D. Wiesler, H. Zabel, and S. M. Shapiro, Physica **B 156–157**, 292 (1989).
9. D. D. Wiesler, H. Zabel, and S. M. Shapiro, Z. f. Physik **B 93**, 277 (1994).
10. A. Hubert and R. Schäfer, *Magnetic domains* (Springer–Verlag, Berlin, 1998).
11. R. Skomski, J. Phys. **C 15**, R841 (2003), URL http://dx.doi.org/10.1088/0953-8984/15/20/202.
12. R. P. Cowburn, J. Magn. Magn. Mater. **242-245**, 505 (2002), URL http://dx.doi.org/10.1016/S0304-8853(01)01086-1.
13. K. Y. Guslienko, V. Novosad, Y. Otani, H. Shima, and K. Fukamichi, Phys. Rev. B 65, 024414 (2001), URL http://dx.doi.org/10.1103/PhysRevB.**65**.024414.
14. T. Shinjo, T. Okuno, R. Hassdorf, K. Shigeto, and T. Ono, Science **289**, 930 (2000).
15. R. P. Cowburn, A. O. Adeyeye, and M. E.Welland, Phys. Rev. Lett. **81**, 5414 (1998), URL http://link.aps.org/abstract/PRL/v81/p5414.
16. R. P. Cowburn, D. K. Koltsov, A. O. Adeyeye, and M. E. W. and D. M. Tricker, Phys. Rev. Lett. **83**, 1042 (1999).
17. R. Pulwey, M. Rahm, J. Biberger, and D. Weiss, IEEE transactions on magnetics **37**, 2076 (2001).
18. G. Gubbiotti, G. Carlotti, F. Nizzoli, RobertoZivieri, T. Okuno, and T. Shinjo, IEEE Transactions On Magnetics **38**, 2532 (2002), URL http://dx.doi.org/10.1109/TMAG.2002. 801920.
19. J. P. Park, P. Eames, D. M. Engebretson, J. Berezovsky, and P. A. Crowell, Phys. Rev. B **67**, 020403 (2003), URL http://link.aps.org/abstract/PRB/v67/e020403.
20. A. Fernandez and C. J. Cerjan, J. Appl. Phys. **87**, 1395 (2000), URL http://link.aip.org/link/?JAP/87/1395/1.
21. J. Raabe, R. Pulwey, R. Sattler, T. Schweiboeck, J. Zweck, and D. Weiss, J. Appl. Phys. **88**, 4437 (2000).
22. A. Lebib, S. P. Li, M. Natali, and Y. Chen, J. Appl. Phys. **89**, 3892 (2001), URL http://link.aip.org/link/?JAP/89/3892/1.
23. M. Schneider, H. Hoffmann, and J. Zweck, Appl. Phys. Lett. **77**, 2909 (2000), URL http://link.aip.org/link/?APL/77/2909/1.
24. S. O. Demokritov, B. Hillebrands, and A. N. Slavin, Physics Reports **348**, 441 (2001), URL http://www.sciencedirect.com/science/article/B6TVP-43B29GN-1/2/92cce5adca2ce19b207e73-d018666fcf.
25. B. Hillebrands and K. Ounadjela, eds., *Spin dynamics in confined magnetic structures*, vol. 83 of *Topics in Applied Physics* (Springer, Berlin, 2002).
26. M. Buess, R. Hŏllinger, T. Haug, K. Perzlmaier, U. K. D. Pescia, M. R. Scheinfein, D.Weiss, and C. H. Back, Phys. Rev. Lett. **93**, 077207 (2004), URL http://dx.doi.org/10.1103/PhysRevLett.93.077207.
27. S. B. Choe, Y. Acremann, A. Scholl, A. Bauer, A. Doran, J.Stŏhr, and H. A. Padmore, Science **304**, 420 (2004).
28. Y. Tserkovnyak, A. Brataas, G. E.W. Bauer, and B. I. Halperin, Rev. Mod. Phys. **77**, 1375 (pages 47) (2005), URL http://link.aps.org/abstract/RMP/v77/p1375.

29. S. D. Bader, Rev. Mod. Phys. **78**, 1 (pages 15) (2006), URL http://link.aps.org/abstract/RMP/v78/p1.
30. J. C. Slonczewski, J. Magn. Magn. Mater. **159**, L1 (1996), URL http://dx.doi.org/10.1016/0304-8853(96)00062-5.
31. L. Berger, Phys. Rev. B **54**, 9353 (1996), URL http://link.aps.org/abstract/PRB/v54/p9353.
32. M. Tsoi, A. G. M. Jansen, J. Bass, W.-C. Chiang, M. Seck, V. Tsoi, and P. Wyder, Phys. Rev. Lett. **80**, 4281 (1998), URL http://dx.doi.org/10.1103/PhysRevLett.80.4281.
33. E. B. Myers, D. C. Ralph, J. A. Katine, R. N. Louie, and R. A. Buhrman, Science **285**, 867 (1999), URL http://dx.doi.org/10.1126/science.285.5429.867.
34. I. N. Krivorotov, N. C. Emley, J. C. Sankey, S. I. Kiselev, D. C. Ralph, and R. A. Buhrman, Science **307**, 228 (2005), URL http://dx.doi.org/10.1126/science.1105722.
35. C. H. Marrows, Advances in Physics **54**, 585 (2005), ISSN 0001-8732, URL http://www.informaworld.com/10.1080/00018730500442209.
36. S. Kasai, Y. Nakatani, K. Kobayashi, H. Kohno, and T. Ono, Phys. Rev. Lett. **97**, 107204 (pages 4) (2006), URL http://link.aps.org/abstract/PRL/v97/e107204.
37. V. S. Pribiag, I. N. Krivorotov, G. D. Fuchs, P. M. Braganca, O. Ozatay, J. C. Sankey, D. C. Ralph, and R. A. Buhrman, Nat Phys **3**, 498 (2007), ISSN 1745-2473, URL http://dx.doi.org/10.1038/nphys619.
38. J.-G. Caputo, Y. Gaididei, F. G. Mertens, and D. D. Sheka, Phys. Rev. Lett. **98**, 056604 (pages 4) (2007), URL http://link.aps.org/abstract/PRL/v98/e056604.
39. D. D. Sheka, Y. Gaididei, and F. G. Mertens, Appl. Phys. Lett. **91**, 082509 (2007), URL http://link.aip.org/link/?APL/91/082509/1.
40. K. Yamada, S. Kasai, Y. Nakatani, K. Kobayashi, H. Kohno, A. Thiaville, and T. Ono, Nat Mater **6**, 270 (2007), ISSN 1476-1122, URL http://dx.doi.org/10.1038/nmat1867.
41. R. P. Cowburn, Nat Mater **6**, 255 (2007), ISSN 1476-1122, URL http://dx.doi.org/10.1038/nmat1877.
42. I. Zutic, J. Fabian, and S. D. Sarma, Rev. Mod. Phys. **76**, 323 (pages 88) (2004), URL http://link.aps.org/abstract/RMP/v76/p323.
43. D. Houssameddine, U. Ebels, B. Delaet, B. Rodmacq, I. Firastrau, F. Ponthenier, M. Brunet, C. Thirion, J.-P.Michel, L. Prejbeanu-Buda, et al., Nat Mater **6**, 447 (2007), ISSN 1476-1122, URL http://dx.doi.org/10.1038/nmat1905.
44. B. A. Ivanov and C. E. Zaspel, Appl. Phys. Lett. **81**, 1261 (2002), URL http://dx.doi.org/10.1063/1.1499515.
45. A. D. Kent, B. Ozyilmaz, and E. del Barco, Appl. Phys. Lett. **84**, 3897 (2004), URL http://link.aip.org/link/?APL/84/3897/1.
46. A. D. Kent, Nat Mater **6**, 399 (2007), ISSN 1476-1122, URL http://dx.doi..org/10.1038/nmat1917.
47. H. Xi, K.-Z. Gao, and Y. Shi, J. Appl. Phys. **97**, 044306 (pages 4) (2005), URL http://link.aip.org/link/?JAP/97/044306/1.
48. A. I. Akhiezer, V. G. Bar'yakhtar, and S. V. Peletminskiĭ, *Spin waves* (North–Holland, Amsterdam, 1968).
49. Z. Li and S. Zhang, Phys. Rev. Lett. **92**, 207203 (pages 4) (2004), URL http://link.aps.org/abstract/PRL/v92/e207203.
50. J. Shibata, Y. Nakatani, G. Tatara, H. Kohno, and Y. Otani, Phys. Rev. B **73**, 020403 (pages 4) (2006), URLhttp://link.aps.org/abstract/PRB/v73/e020403.
51. Y. Liu, S. Gliga, R. Hertel, and C. M. Schneider, Appl. Phys. Lett. **91**, 112501 (pages 3) (2007), URLhttp://link.aip.org/link/?APL/91/112501/1.
52. A. Aharoni, J. Appl. Phys. **68**, 2892 (1990), URL http://link.aip.org/link/?JAP/68/2892/1.
53. C. A. Ross, M. Hwang, M. Shima, J. Y. Cheng, M. Farhoud, T. A. Savas, H. I. Smith,W. Schwarzacher, F. M.Ross, M. Redjdal, et al., Phys. Rev. B **65**, 144417 (2002), URL http://link.aps.org/abstract/PRB/v65/e144417.

54. K. Y. Guslienko and V. Novosad, J. Appl. Phys. **96**, 4451 (2004), URL http://link.aip.org/link/?JAP/96/4451/1.
55. J.-G. Caputo, Y. Gaididei, V. P. Kravchuk, F. G. Mertens, and D. D. Sheka, Phys. Rev. B **76**, 174428 (pages 13)(2007), URL http://link.aps.org/abstract/PRB/v76/e174428.
56. K. Y. Guslienko and A. N. Slavin, Phys. Rev. B **72**, 014463 (pages 5) (2005), URL http://link.aps.org/abstract/PRB/v72/e014463.
57. N. A. Usov and L. G. Kurkina, J. Magn. Magn. Mater. **242-245**, 1005 (2002), URL http://www.sciencedirect.com/science/article/B6TJJ-44SKJ302/2/a46025775c4633f795d346427-c44d37.
58. A. A. Thiele, Phys. Rev. Lett. **30**, 230 (1973), URL http://link.aps.org/abstract/PRL/v30/p230.
59. A. A. Thiele, J. Appl. Phys. **45**, 377 (1974), URL http://link.aip.org/link/?JAP/45/377/1.
60. D. L. Huber, Phys. Rev. B **26**, 3758 (1982), URL http://link.aps.org/abstract/PRB/v26/p3758.
61. A. V. Nikiforov and É. B. Sonin, Soviet Physics - JETP 58, 373 (1983), URL http://link.aip.org/ link/?SPJ/58/373/1.
62. K. Y. Guslienko, B. A. Ivanov, V. Novosad, Y. Otani, H. Shima, and K. Fukamichi, J. Appl. Phys. **91**, 8037 (2002), URL http://link.aip.org/link/?JAP/91/8037/1.
63. S. Savel'ev and F. Nori, Phys. Rev. B **70**, 214415 (pages 19) (2004), URL http://link.aps.org/abstract/PRB/v70/e214415.
64. K. Y. Guslienko, X. F. Han, D. J. Keavney, R. Divan, and S. D. Bader, Phys. Rev. Lett. **96**, 067205 (pages 4) (2006), URL http://link.aps.org/abstract/PRL/v96/e067205.
65. B. A. Ivanov and C. E. Zaspel, J. Appl. Phys. **95**, 7444 (2004), URL http://dx.doi.org/10.1063/1.1652420.
66. C. E. Zaspel, B. A. Ivanov, J. P. Park, and P. A. Crowell, Phys. Rev. B **72**, 024427 (2005), URL http://dx.doi.org/10.1103/PhysRevB.72.024427.
67. Y. Liu, H. He, and Z. Zhang, Appl. Phys. Lett. **91**, 242501 (pages 3) (2007), URL http://link.aip.org/link/?APL/91/242501/1.
68. B. A. Ivanov and C. E. Zaspel, Phys. Rev. Lett. **99**, 247208 (pages 4) (2007), URL http://link.aps.org/abstract/PRL/v99/e247208.
69. V. B. Waeyenberge, A. Puzic, H. Stoll, K. W. Chou, T. Tyliszczak, R. Hertel, M. Fähnle, H. Bruckl, K. Rott, G. Reiss, et al., Nature **444**, 461 (2006), ISSN 0028-0836, URL http://dx.doi.org/10.1038/nature05240.
70. Q. F. Xiao, J. Rudge, B. C. Choi, Y. K. Hong, and G. Donohoe, Applied Physics Letters **89**, 262507 (pages 3)(2006), URL http://link.aip.org/link/?APL/89/262507/1.
71. R. Hertel, S. Gliga, M. F¨ahnle, and C. M. Schneider, Phys. Rev. Lett. **98**, 117201 (pages 4) (2007), URLhttp://link.aps.org/abstract/PRL/v98/e117201.
72. K.-S. Lee, K. Y. Guslienko, J.-Y. Lee, and S.-K. Kim, Phys. Rev. B **76**, 174410 (pages 5) (2007), URLhttp://link.aps.org/abstract/PRB/v76/e174410.
73. V. P. Kravchuk, D. D. Sheka, Y. Gaididei, and F. G. Mertens, J. Appl. Phys. **102**, 043908 (2007), URLhttp://link.aip.org/link/?JAP/102/043908/1.
74. S. Komineas and N. Papanicolaou, in *Electromagnetic, magnetostatic, and exchange-interaction vortices inconfined magnetic structures*, edited by E. Kamenetskii (RESEARCH SIGNPOST, 2008).
75. S. Komineas, Phys. Rev. Lett. **99**, 117202 (pages 4) (2007), URL http://link.aps.org/abstract/PRL/v99/e117202.
76. A. A. Belavin and A. M. Polyakov, JETP Lett. **22**, 245 (1975).
77. R. Hertel and C. M. Schneider, Phys. Rev. Lett. **97**, 177202 (pages 4) (2006), URL http://link.aps.org/abstract/PRL/v97/e177202.
78. O. A. Tretiakov and O. Tchernyshyov, Phys. Rev. B **75**, 012408 (pages 2) (2007), URL http://link.aps.org/abstract/PRB/v75/e012408.
79. *MapleSoft*, URL http://www.maplesoft.com.